Science of the Total Environment 887 (2023) 163938

Contents lists available at ScienceDirect

Science of the Total Environment

journal homepage: www.elsevier.com/locate/scitotenv

Enabling circular economy by N-recovery: Electrocatalytic reduction of nitrate with cobalt hydroxide nanocomposites on copper foam treating low conductivity groundwater effluents

Gabriel Antonio Cerrón-Calle [a], Ana S. Fajardo [a,b,c], Jingyue Liu [d], Carlos M. Sánchez-Sánchez [b], Sergi Garcia-Segura [a,*]

[a] Nanosystems Engineering Research Center for Nanotechnology-Enabled Water Treatment, School of Sustainable Engineering and the Built Environment, Arizona State University, Tempe, AZ 85287-3005, USA
[b] Sorbonne Université, CNRS, Laboratoire Interfaces et Systèmes Electrochimiques (LISE), 4 place Jussieu, F-75005 Paris, France
[c] Polytechnic Institute of Coimbra, Applied Research Institute, Rua da Misericórdia, Lagar dos Cortiços – S. Martinho do Bispo, 3045-093 Coimbra, Portugal
[d] Department of Physics, Arizona State University, Tempe, AZ 85287-1504, USA

HIGHLIGHTS

- Electrodeposition time controls the surface coverage of Cu/Co(OH)$_x$ catalyst.
- Cu/Co(OH)$_x$ produces more than pristine Cu foam: 0.7vs0.3 mmol NH_3 g_{cat}^{-1} h^{-1}.
- Co(OH)x sites demonstrated catalytic hydrogenation experimentally.
- Bimetallic electrode demonstrated high catalytic stability after 12 h.

GRAPHICAL ABSTRACT

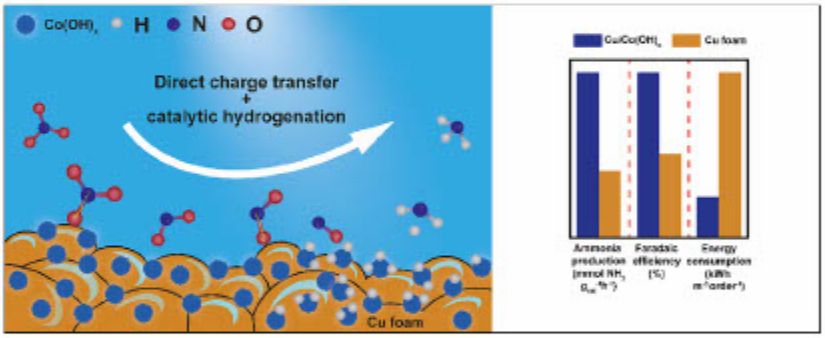

ARTICLE INFO

Editor: Damia Barcelo

Keywords:
Electrochemical water treatment
Nitrogen cycle
Bimetallic catalysts
Non-platinum group metals (non-PGMs)
Hydrogenation
Green chemistry

ABSTRACT

Fertilizers play a vital role in the food-energy-water nexus. The traditional method of artificial nitrogen fixation to produce ammonia is a high-energy intensive centralized process that has caused an imbalance of the N-cycle due to the release of N-species to water. Electrocatalytic nitrate reduction (ENR) to ammonia is a promising N-resource recovery alternative that can enable the circular reuse of ammonia in decentralized settings. However, the primary challenge is identifying selective and affordable electrocatalysts. Identifying electrodes that rely on something other than platinum-group metals is required to surpass barriers associated with using expensive and endangered elements. In this study, an earth-abundant bimetallic catalyst, Cu/Co(OH)$_x$, prepared and optimized by electrodeposition, demonstrates superior ammonia production. Under environmentally relevant conditions of 30 mg NO_3^--N L^{-1}, Cu/Co(OH)$_x$ showed higher ammonia production than pristine Cu foam with 0.7 and 0.3 mmol NH_3 g_{cat}^{-1} h^{-1}, respectively. The experimental evaluation demonstrated direct reduction and catalytic hydrogenation mechanisms in Cu/Co(OH)$_x$ sites. Leaching analyses suggest that Cu/Co(OH)$_x$ has outstanding stability with negligible metal concentration below the maximum contaminant level for both Cu and Co. These results provide a framework for using earth-abundant materials in ENR with comparable efficiency and energy consumption to platinum-group materials.

* Corresponding author.
E-mail address: Sergio.garcia.segura@asu.edu (S. Garcia-Segura).

http://dx.doi.org/10.1016/j.scitotenv.2023.163938
Received 1 March 2023; Received in revised form 29 April 2023; Accepted 30 April 2023
Available online 05 May 2023

1. Introduction

Nitrate (NO_3^-) is considered one of the top 10 drinking water pollutants in the United States (Glenn and James Lester, 2010; Liu et al., 2005), as a result of the widespread anthropogenic release of N-species into water from the use of fertilizers. The World Health Organization established a maximum contamination level (MCL) of 10 mg NO_3^--N L^{-1} because above this nitrate concentration serious health risks can result, such as respiratory and reproductive system illness, thyroid problems, cancer, and even death (Singh et al., 2022; Teng et al., 2019). To mitigate the nitrate pollution, the electrochemical reduction process has emerged as a promising technology not only to remove the pollutant but at the same time to enable nitrogen resource recovery of an added-value product, as is the case of ammonia (Katsounaros, 2021; Lin et al., 2019; Liu et al., 2020; Marcos-Hernández et al., 2022; Tucker et al., 2004; Wang et al., 2020a). An additional advantage is that electrified systems can be deployed holistically anywhere as decentralized technologies operated by renewable energies (dos Santos et al., 2023; van Langevelde et al., 2021). These advances may circumvent the use of the conventional Haber-Bosch process in the synthesis of ammonia which is responsible for over 450 million tons of CO_2 emission annually (~ 1.2 % of global greenhouse gas emissions) (Juangsa et al., 2021; MacFarlane et al., 2020). The electrochemical reduction of nitrate (ERN, Eq. (1)) combined with a renewable electricity source appears as a fossil fuel-free technology to produce ammonia under ambient conditions.

$$NO_3^- + 9H^+ + 8e^- \rightarrow NH_3 + 3H_2O \quad (1)$$

The main barrier to ERN is the reliance on monometallic electrocatalysts from the platinum group metals (PGMs). Research has chiefly focused on studying platinum and palladium as noble cathodic PGMs because of their high electrocatalytic activity and corrosion resistance (Gauthard et al., 2003; Guo et al., 2022; Hasnat et al., 2014; Lotfi et al., 2020; Shen et al., 2020). The use of Pt and Pd electrodes on a large scale exerts severe technology translation limitations, since their cost directs the capital expenditure of systems (Flores et al., 2022). Life cycle assessments suggest that extensive use of these endangered elements (i.e., PGMs) is not feasible (Price, 2011). Thus, reducing the amount of these metals in the catalytic material or identifying alternative catalytic materials is required to ensure competitive deployment of ERN as a dual water treatment and resource recovery technology.

Bimetallic electrodes can synergistically boost the performance of abundant transition metals (i.e., Fe, Co, Ni, Cu, Zn) through the formation of hybrid metal interfaces and metal/metal-oxides as catalytic sites (Barley et al., 1986; Cerrón-Calle et al., 2023; Fajardo et al., 2021; Hamid et al., 2020; Jung et al., 2009; Shen et al., 2020; Wu et al., 2021). Indeed, combining different metal catalytic sites that play different specific roles has proven to be a successful approach (Hao et al., 2022; Yang et al., 2022). For example, our group has already published Cu electrodes decorated with electrodeposited nanodomains of Pt (< 0.5 wt%), which displayed increased ammonia yields 194.4 mg L^{-1} g_{cat}^{-1} NH_3-N in Cu-Pt by combining charge transfer and hydrogenation mechanisms enabled by Cu and Pt, respectively (Cerrón-Calle et al., 2022). Other metals different than PGMs are prone to form metal hydroxide or oxide interfaces (i.e., Fe, Co, etc.) (Deng et al., 2021; Jonoush et al., 2020). Cobalt has been identified as a competitive monometallic catalyst for ERN, while bimetallic cobalt-containing electrodes and particularly Cu-Co have demonstrated efficient nitrate removal and ammonia production (Fu et al., 2023; He et al., 2022; Li et al., 2022; Niu et al., 2022b, 2022a; Wang et al., 2023; Wu et al., 2022). According to density functional theory (DFT) findings, Co sites increase the energy required to overcome the barrier to form H_2 while favoring monoatomic H* adsorption and stabilization (Cui et al., 2017; Liu et al., 2021; Xu et al., 2021; Yu et al., 2020). This H* presents a strong reducing environment with an E° (H^+/H*) = −2.3 V vs SHE that could be potentially exploited to steep the nitrate reduction to ammonia (Garcia-Segura et al., 2018; Tucker et al., 2004). Ammonia production is represented by ammonia yield (mmol NH_3 g_{cat}^{-1} h^{-1}), which may depend on the initial nitrogen content. For example, the same electrode using different initial nitrate concentrations can obtain different ammonia yields since it can affect the surface coverage ratio between adsorbed N-species and monoatomic hydrogen. Thereby, it is relevant to consider closer to realistic conditions when benchmarking electrocatalytic materials and this is the reason why we study low conductivity and low nitrate content effluents (Garcia-Segura et al., 2020).

This work aims to pave the way towards the identification of alternative earth-abundant catalysts under environmentally representative nitrate conditions that may outperform conventional PGMs not only in cost competitiveness but also in overall performance and selectivity. Although some works have been recently published regarding the synergy between copper and cobalt as electrodes for the ERN (Fu et al., 2023; He et al., 2022; Li et al., 2022; Niu et al., 2022a, 2022b; Wang et al., 2023; Wu et al., 2022), to the best of our knowledge little has been explored in terms of 3D materials and the use of galvanostatic conditions that are the most adequate for the scalability of real systems. The new electrosynthesized electrodes (Cu foam/Co(OH)$_x$) working under galvanostatic conditions and using a low conductivity and low nitrate content effluent were benchmarked against the bare Cu foam and our previous work using Cu foam-Pt in terms of ERN kinetics conversion, product selectivity, and engineering figures of merit. However, no other single example of Cu-Co electrodes working under galvanostatic conditions were found in the literature for the sake of comparison. In addition to this, Cu/Co(OH)$_x$ electrode stability was assessed through a sequential fed batch trial and metal leaching in solution was quantified. The synergetic behavior of the cobalt-copper interfaces demonstrated superior electrocatalytic outcomes and signaled this type of PGM-free electrodes for sustainable environmental protection and resource recovery in the circular economy.

2. Materials and methods

2.1. Chemicals and materials

Ultrapure water was used for all solutions with resistivity >18.2 MΩ cm at 25 °C provided by Elga Water. Sodium sulfate (Na_2SO_4) of analytical grade (≥ 99.0 %) purchased from Sigma-Aldrich was used as a supporting electrolyte. Individual solutions containing inorganic nitrogen species supplied by Sigma-Aldrich were prepared with analytical grade (≥ 99.0 %): sodium nitrate ($NaNO_3$), sodium nitrite ($NaNO_2$), and ammonium sulfate ($(NH_4)_2SO_4$). Ter-butyl alcohol (≥ 99 %, Sigma-Aldrich) was used as atomic hydrogen scavenger. Copper foam (110 pores per inch, 1.5 × 1.5 cm^2, 2 mm thick, area density ≈ 330 g m^2) with 99.99 % purity was purchased from Futt and used as a 3D electrode. Electrodes were modified with cobalt nanocomposites by using ($CoSO_4{\cdot}6H_2O$, ≥ 99.0 %) and boric acid (H_3BO_3, ≥ 99.5 %) acquired from Sigma-Aldrich. Acetone ($(CH_3)_2CO$, ≥ 99.5 %) and hydrochloric acid (HCl, ≥ 37.0 %), provided by Sigma-Aldrich, were used for copper surface pre-treatment.

2.2. Electrodeposition of Co(OH)x nanocomposites over Cu substrate

The electrodeposition of Co(OH)$_x$ nanocomposites over Cu foam electrodes was performed by chronoamperometry using the PGSTAT302N (Metrohm, USA) potentiostat. To remove surface impurities, Cu foams were pre-treated by sonicating them in acetone for 15 min to remove organic compounds and greases, sank in 1.0 mol L^{-1} HCl for 5 min, thoroughly rinsed with ultrapure water, and dried at room temperature. The electrodeposition was conducted in a three-electrode cell using Ag/AgCl (3.5 M KCl) as the reference electrode, platinum plate as the counter-electrode, and Cu foam as the working electrode. The electrodeposition bath consisted of 10 mmol L^{-1} $Co(SO_4)_2{\cdot}6H_2O$, 0.5 mol L^{-1} H_3BO_3, and 0.1 mol L^{-1} Na_2SO_4 with a final pH of 4.5. The working electrode underwent cathodic polarization conditions at −1.2 V vs Ag/AgCl, based on the cyclic voltammetry Fig. S1, during 60, 120, 180, and 360 s. Then, the mass of the dried electrode was registered. According to Fig. S2, the electrosynthesis of the Cu/Co(OH)$_x$ at 180 s presented the higher nitrate conversion, being therefore selected for the following tests.

2.3. Characterization of three-dimensional electrodes

The morphology and elemental analysis were carried out by field emission scanning electron microscope coupled with energy-dispersive X-ray spectroscopy (FESEM-EDS), Auriga-Zeiss. Cu foam crystallographic information was evaluated by X-ray diffraction (XRD) using a PANanalytical Aeris diffractometer with Cu (Kα = 1.5406 Å) radiation source (45 kV and 30 mA) from 20° to 80°. The crystallographic structure of cobalt composites was evaluated on an aberration-corrected (scanning) transmission electron microscope (STEM) (JEM-ARM200F) with a nominal resolution of 0.08 nm. Before STEM examination, the bimetallic electrode was ultrasonically dispersed in ethanol, and a drop of the solution was cast onto a lacey carbon-coated TEM grid. X-ray photoelectron spectroscopy analyses were performed using a Kratos AXIS Supra+ with a monochromatic Al Kα ion beam (beam energy = 1486.6 eV).

In a conventional three-electrode system, the electrochemical characterization was carried out by linear sweep voltammetry (LSV) and cyclic voltammetry (CV). The three-electrode system was set up using Cu foam (modified or pristine) as the working electrode, Ag/AgCl (3.5 mol L^{-1} KCl) as the reference electrode, and a Pt plate as the counter electrode. The geometrical area was determined considering the areal density and the mass registered (4.5 cm^2) and used to define current density. Solutions were deaerated with Ar before carrying out electrochemical measurements to ensure the absence of oxygen dissolved in the electrolyte.

The electrochemical surface area (ECSA) was evaluated in a solution of 0.1 mol L^{-1} Na_2SO_4 at different scan rates (75, 50, 25, 10, and 5 mV s^{-1}) using Eq. (2).

$$ECSA = \frac{C_{dl}}{C_s} \tag{2}$$

Where C_{dl} is the double-layer capacitance, and C_s is related to the specific capacitance of the sample. The value of C_{dl} was calculated experimentally using Eq. (3).

$$C_{dl} = \frac{i_c}{v} \tag{3}$$

Where i_c is the charging current and v is the scan rate. Then, plotting the values of i_c vs v using a linear fitting, the value of C_{dl} is associated with the curve slope. A general value for C_s = 0.040 mF cm^{-2} was used to estimate the ECSA, as reported by several studies (Li et al., 2020; Wang et al., 2020b).

The electrochemical behavior and direct electron transfer for ERN of each electrode were studied by linear sweep voltammetry (LSV). LSV was performed at 10 mV s^{-1} in solutions of 0.1 mol L^{-1} Na_2SO_4 as support electrolyte in the presence or absence of 20 mmol L^{-1} nitrogen oxyanions (i.e., $NaNO_3$ or $NaNO_2$) to assign reduction peaks.

Hydrogen adsorption was evaluated on the electrode surface by CV using bimetallic configurations Cu/Co$(OH)_x$ (180 s) as the working electrode, Hg/HgO (1.0 mol L^{-1} NaOH) as the reference electrode, and Pt plate as the counter electrode. CV was recorded at 25 mV s^{-1} in solutions of 0.1 mol L^{-1} NaOH at different reduction limits (−1.0, −1.2, and -1.4 V vs Hg/HgO). All potentials used are referenced to a reversible hydrogen electrode (RHE), according to Eq. (4) and Eq. (5). Where $E°_{Ag/AgCl}$ and $E°_{Hg/HgO}$ are 197 mV and 98 mV at 25 °C, respectively.

$$E(RHE) = E°_{Ag/AgCl} + 0.059\,pH + E_{Ag/AgCl} \tag{4}$$

$$E(RHE) = E°_{Hg/HgO} + 0.059\,pH + E_{Hg/HgO} \tag{5}$$

2.4. Electrochemical reduction of nitrate

The electrocatalytic reduction of nitrate was carried out in an open batch reactor at 25 °C using 100 mL of non-deaerated 30 mg L^{-1} NO_3^--N (2.1 mM NO_3^-) solution with 12.5 mmol L^{-1} Na_2SO_4, which correspond to contaminated natural groundwater effluents (Atrashkevich et al., 2022). Electrolysis was conducted under magnetic stirring at 500 rpm to ensure mass transfer. The initial pH and conductivity conditions were 5.90 ± 0.2 and 3.20 ± 0.05 mS cm^{-1}, respectively. All experiments were operated under galvanostatic conditions using the power supply TENMA 72–2720 DC at 20 mA cm^2. The Cu foam and Cu/Co$(OH)_x$ were used as cathodes (geometrical area = 4.5 cm^2, electrode mass = 0.15 g), and commercial Ti/IrO_2 (DeNora – USA) as an anode in a two-electrode system. Blank re-oxidation experiments were performed using 30 mg L^{-1} NO_2^--N or 30 mg L^{-1} NH_3-N in 12.5 mmol L^{-1} Na_2SO_4. Aliquots of ~2.0 mL were withdrawn as samples at specific electrolysis times during the 120 min of treatment to analyze NO_3^--N, NO_2^--N, and NH_3-N. All the ERN experiments were performed in triplicate and deviations between them were lower than 5 % for all trials.

2.5. Analytical instruments and performance evaluation

Thermo Scientific Orion Star A221 meters were used to assess the pH and conductivity. Nitrate (mg NO_3^--N L^{-1}), nitrite (mg NO_2^--N L^{-1}), and ammonia (mg NH_3-N L^{-1}) concentrations were spectrophotometrically analyzed over time by a UV–vis spectrophotometer model DR6000 (HACH) using commercially available colorimetric kits TNT 835 (λ = 345 nm), TNT 839 (λ = 515 nm) and TNT 830 (λ = 694 nm) from HACH, respectively. The nitrate conversion was calculated using Eq. (6)

$$Nitrate\ conversion\ (\%) = \frac{C_{nitrate,i} - C_{nitrate,t}}{C_{nitrate,i}} \times 100 \tag{6}$$

$C_{nitrate,i}$ is the nitrate concentration in mg NO_3^--N L^{-1} before treatment, and $C_{nitrate,t}$ is the nitrate concentration at time (t). N-volatile species (N_2, NO, NO_2, or N_2O) were determined by the mass balance on aqueous nitrogen species and labeled as N-gas. The ammonia yield can be calculated using Eq. (7)

$$Ammonia\ yield\ \left(mmol\ NH_3\ g_{cat}^{-1}\ h^{-1}\right) = \frac{C_{NH_3} V}{m_{cat} t} \tag{7}$$

Where C_{NH_3} is the ammonia concentration (mmol L^{-1}), V is the volume of the solution (L), m_{cat} is catalyst mass (g), and t is time (h).

The product selectivity towards ammonia (S_{NH_3}) was calculated from Eq. (8), and the percentage of ammonia conversion can be estimated by Eq. (9). The selectivity describes the rate at which desired product ammonia has been electrogenerated from the reduced nitrate. The percentage of ammonia production illustrates the amount of ammonia electrogenerated concerning the theoretical maximum expected defined by the initial nitrate concentration in the solution. Note that the ammonia production percentage provides a more critical engineering metric for efficient recovery of added value resources that reflects both selectivity aspects and conversion attained during the treatment time.

$$S_{NH_3}(\%) = \frac{C_{NH_3,exp}}{C_{nitrate,i} - C_{nitrate,t}} \times 100 \tag{8}$$

$$Ammonia\ production\ (\%) = \frac{C_{NH_3,exp}}{C_{NH_3,theo}} \times 100 \tag{9}$$

Where $C_{NH_3,exp}$ is the concentration of ammonia experimentally obtained (mg NH_3-N L^{-1} in S_{NH_3} and mmol in *ammonia production*), $C_{nitrate,i}$ is the nitrate concentration in mg NO_3^--N L^{-1} before treatment, and $C_{nitrate,t}$ is the nitrate concentration in mg NO_3^--N L^{-1} at time t, and $C_{NH_3,theo}$ is the ammonia concentration in mmol obtained if all the initial nitrate would be converted in ammonia. The Faradaic efficiency (FE) estimated from Eq. (10) was used as a figure of merit that determines the performance of the system from the number of electrons consumed in an electrochemical reaction relative to the expected theoretical conversion ruled by Faraday's law.

$$FE(\%) = \frac{nFN_i}{3600It} \times 100 \tag{10}$$

Where n is the number of electrons required per mol of ammonia (mol), F is the Faraday constant (96,485 C mol^{-1}), N_i is the mol of ammonia generated during the electrolysis, I is the applied electric current (A), t is the electrolysis time (h), and 3600 is a unit conversion factor (3600 s h^{-1}).

Electrical energy per order (*EE/O*) was used as an engineering figure of merit to benchmark the electric energy required to reduce NO_3^--N concentration by one order of magnitude in a unit volume calculated from Eq. (11) for batch operation mode.

$$EE/O\left(kWh\ m^{-1}order^{-1}\right) = \frac{ItE_{cell}}{V_s \log C_{nitrate,i}/C_{nitrate,f}} \times 100 \quad (11)$$

Where E_{cell} is the average of the cell potential (V), I is the current intensity (A), t is the time (h), V_s is the solution volume (L), and $C_{nitrate,i}$ and $C_{nitrate,f}$ are the initial and final concentration after one-order of magnitude reduction of nitrate.

Metal leaching was recorded by induced coupled plasma with mass spectrometry (ICP-MS, Perkin Elmer) after each treatment period (120 min) during six cycles with the same electrode. The obtained calibration curves has a correlation factor of 0.99 or higher for the analysis of Cu and Co.

3. Results and discussion

3.1. Physical characterization of three-dimensional Cu and Cu/Co(OH)$_x$ electrodes

The morphological characterization of the pristine Cu foam and the Cu/Co(*OH*)$_x$ nanocomposites was performed by field-emission scanning electron microscope (FE-SEM). As shown in Fig. S3a at 500 X, the morphology of the Cu foam presented a macro-porous three-dimensional arrangement. Additionally, at a higher magnification 10k X, the pristine Cu foam appeared as a smooth surface without any composites (Fig. 1a). Conversely, the Cu/Co(*OH*)$_x$ electrode in Fig. 1b presented modifications on the substrate. In fact, Fig. 1c revealed a porous surface formed by nanoflake-shaped composites on the Cu surface with an average size of around 70 nm. An energy-disperse X-ray spectroscopy (EDS) mapping analysis was performed to the surface of the Cu/Co(*OH*)$_x$ electrode material displaying an elemental composition of Cu, Co, and O (Fig. S3b).

The Cu foam crystal phase was evaluated by X-ray diffraction (Fig. S4) evidencing the crystallographic planes (111), (200), and (220) which correspond with the face centered cubic structure. The XRD pattern of Cu/Co(*OH*)$_x$ did not show any additional peak (Fig. S4), which may be due to the low amount of material present compared to the bulk Cu foam. Furthermore, the high-angle annular dark-field STEM images (Fig. 1d, f) reveal the particle size, morphology, and surface modulations of the particles, and the atomic resolution phase-contrast STEM images for Co(*OH*)$_x$ nanocomposites are illustrated in (Fig. 1e and g). Lattice-resolved phase-contrast STEM of Co(*OH*)$_x$ presented a lattice spacing of 0.24 and 0.27 nm, which correspond to the (101) and (010) planes of $Co(OH)_2$, respectively. Fig. 1e also presents a lattice spacing of 0.22 nm corresponding to the (012) plane of CoOOH. This crystal phase suggests the partial oxidation of $Co(OH)_2$ to CoOOH, resulting in coexisting crystal phases (i.e., $Co(OH)_2$ and CoOOH) on the electrode surface (Roy et al., 2017; Su et al., 2014).

The chemical composition of Cu foam was evaluated before and after the electrodeposition of cobalt nanocomposites by a wide-range XPS (Fig. 2a). Pristine Cu foam showed a defined Cu 2p peak signal and the characteristic peaks of C 1s and O 1s. The XPS spectrum of Cu/Co(*OH*)$_x$

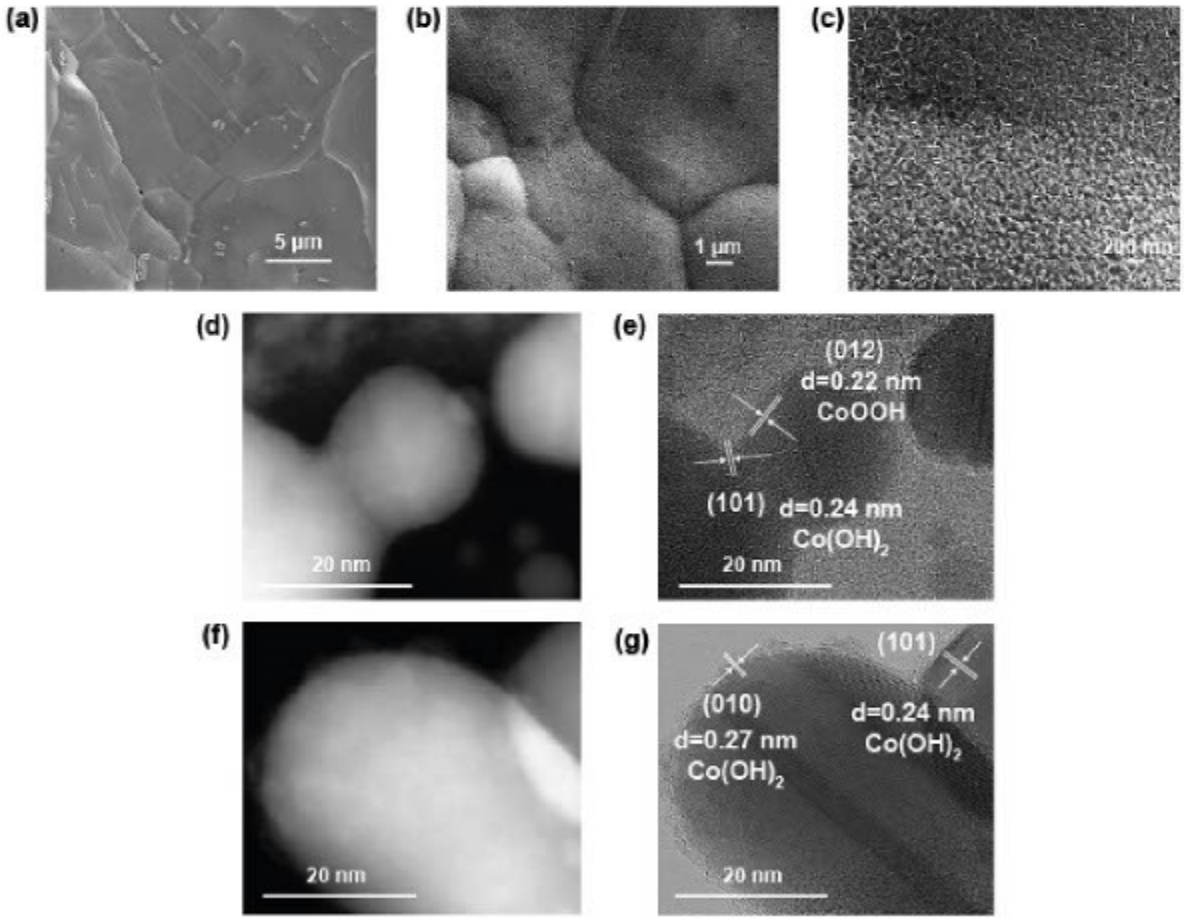

Fig. 1. SEM images of (a) bare Cu foam surface and (b, c) Cu/Co(*OH*)$_x$ surface at different magnifications. (d, f) High-angle annular dark-field STEM images of Cu/Co(*OH*)$_x$ and (e, g) the corresponding atomic resolution phase-contrast STEM images of $Co(OH)_2$ and CoOOH crystals.

(Fig. 2a) presented a Co 2p signal beyond the Cu 2p, C 1s, and O 1s peaks. The low intensity and shift of Cu 2p peaks in the wide-range spectra after electrodeposition suggested an effective superficial coverage of the Cu foam surface. The high-resolution XPS for Cu 2p in Cu foam (Fig. S5a) demonstrated the co-existence of Cu^0, Cu^{1+}, and Cu^{2+}, which will prove the co-existence of pure copper with superficial copper oxide. The difference between Cu^0 and Cu^{1+} is hard to be discerned due to the slight binding energy shift (~0.3 eV) between both species. Thus, the deconvolution of the Cu $2p_{3/2}$ spectrum involved mainly two peaks at 930.9 eV and 932.6 eV that correspond to Cu^0/Cu^{1+} and Cu^{2+}, respectively. Similarly, the Cu $2p_{1/2}$ spectrum consisted of two peaks at 950.8 eV and 952.4 eV, related to Cu^0/Cu^{1+} and Cu^{2+}, respectively (Ivanova et al., 2020; Liang et al., 2023; Ren et al., 2022). The XPS spectra for Cu 2p in Cu/Co$(OH)_x$ (Fig. 2b) presents similar peaks, slightly shifted and with lower intensity than pristine Cu due to Co$(OH)_x$ presence. In Fig. 2c, the Co 2p high-resolution XPS spectrum revealed the presence of both species Co^{2+} and Co^{3+} for the Cu/Co$(OH)_x$ material. In Co $2p_{3/2}$, the peaks at 779.2 eV and 781.6 eV were related to Co^{3+} and Co^{2+}, respectively. Co $2p_{1/2}$ was separated into two peaks for Co^{2+} at 796.2 eV and Co^{3+} at 798.5 eV (Gao et al., 2020; Liu et al., 2021; Roy et al., 2017). This result suggests that the Co$(OH)_x$ is partially oxidized to CoOOH (i.e., Co^{2+} to Co^{3+}), corresponding to the lattice phase identified by STEM images. The O 1 s spectrum was associated with the Cu/Co$(OH)_x$ in Fig. 2d and was deconvoluted into three peaks. The first peak at 530.5 eV (O1) was related to the OH^- group from cobalt hydroxide on the surface (Xiao et al., 2020). The second peak was centered at 531.8 eV (O2) and can be attributed to oxygen vacancy in the structure; this is typically observed in CoOOH structures that enable the formation of a higher oxidation state of cobalt (i.e., Co^{3+}) (Dai et al., 2020; Gao et al., 2022; Xiao et al., 2020). The third peak related to chemisorbed oxygen (O3) was observed at 532.6 eV (Roy et al., 2017). The pristine Cu foam high-resolution spectra of O 1 s (Fig. S5b) showed the same three peaks of oxygen species but with lower intensity, suggesting a lower content of oxygen on the surface.

3.2. Understanding the electrocatalytic properties of Cu/Co$(OH)_x$ using electroanalysis

The electrochemical surface area (ECSA) was estimated for Cu foam and Cu/Co$(OH)_x$ using electrical double layer estimation. It is important to remark that after electrodeposition of Co$(OH)_x$ nanoparticles, the electrochemical surface area (ECSA) decreased from 1.7 m^2 for pristine Cu foam down to 1.2 m^2 for Cu/Co$(OH)_x$, respectively (see Fig. S6). These results demonstrate that the enhanced performance of Cu/Co$(OH)_x$ is not associated with an increase on ECSA but to the unique synergies enabled by Co$(OH)_x$ surface activity.

Electrochemically driven resource recovery approaches from nitrate-polluted wastewater aim to recover ammonia selectively as the final product. The reduction reaction of nitrate initially generates nitrite as stable intermediate species following Eq. (12). Subsequent reduction leads to the formation of ammonia, according to Eq. (13).

$$R_{NO_3^-}: NO_3^- + 2H^+ + 2e^- \rightarrow NO_2^- + H_2O \quad (12)$$

$$R_{NO_2^-}: NO_2^- + 7H^+ + 6e^- \rightarrow NH_3 + 2H_2O \quad (13)$$

To gain mechanistic insight into the charge transfer processes involved at the different electrocatalytic interfaces, linear sweep voltammetry (LSV)

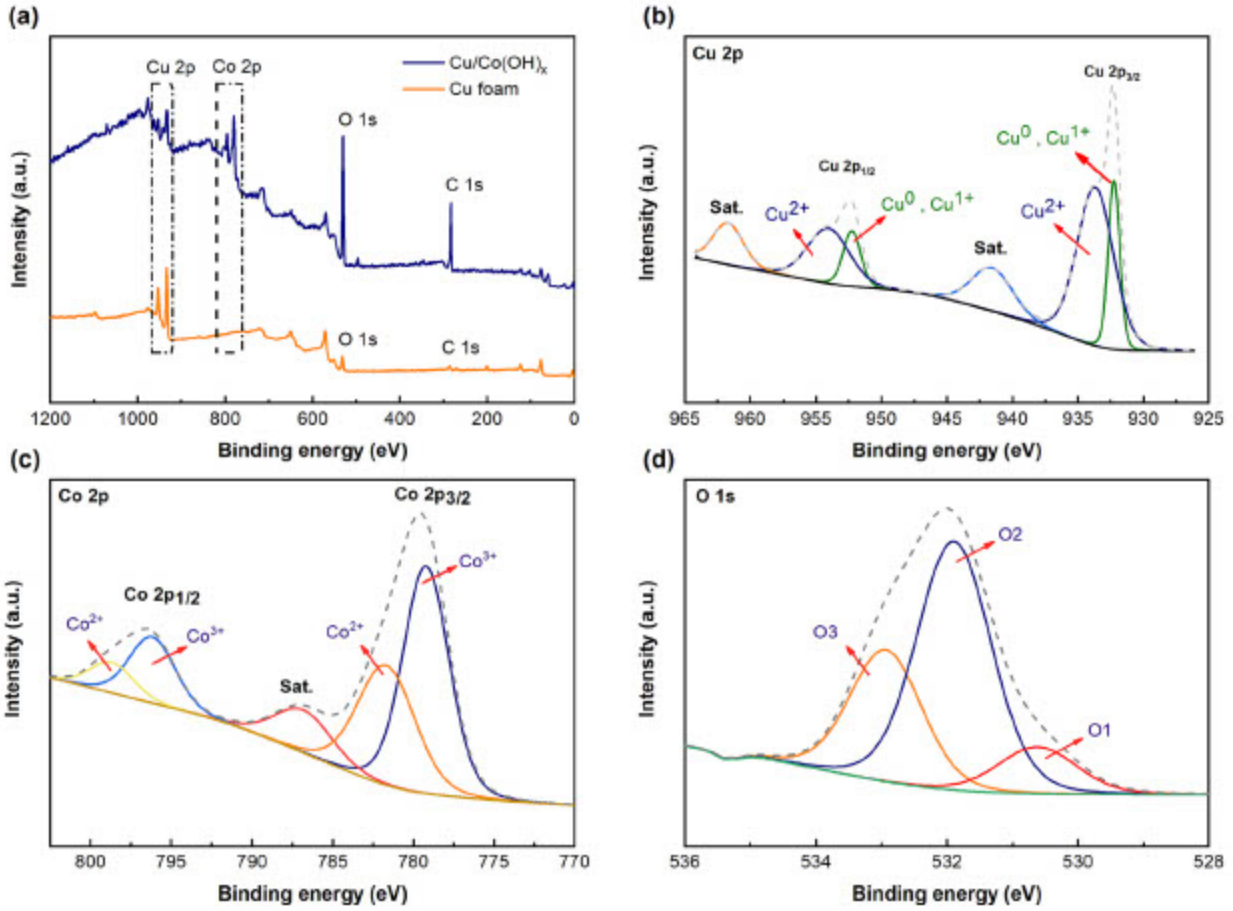

Fig. 2. XPS spectra for Cu foam and Cu/Co$(OH)_x$ electrodes: (a) wide-range spectrum, high-resolution XPS of (b) Cu 2p in Cu/Co$(OH)_x$, (c) Co 2p in Cu/Co$(OH)_x$, and (d) O 1 s in Cu/Co$(OH)_x$.

of a 20 mmol L^{-1} NO_2^- was evaluated first to identify the thermodynamic conditions of Eq. (13) that yields ammonia from nitrite. Fig. 3a illustrates the behavior of pristine Cu and Cu/$Co(OH)_x$ electrodes towards NO_2^- reduction, where a significant increase in the current density response is clearly shown on Cu/$Co(OH)_x$ electrode (blue plot) in comparison with bare Cu electrode (orange plot). This implies a higher electrocatalytic response and an enhanced charge transfer reaction at the nanocomposite electrode interface. Moreover, the comparison between blank and nitrite-containing solutions suggests that nitrite reduction (Eq. (13)) and hydrogen evolution reaction (HER) (Eq. (14)) are competitive processes coexisting under cathodic polarization conditions at the potential range required for ammonia production. In contrast, no significant differences in current response were observed for the LSV of blank solutions using either Cu foam or Cu/$Co(OH)_x$ electrodes.

$$2H_2O + 2e^- \rightarrow H_{2(g)} + 2OH^- \quad (14)$$

The LSV of NO_3^- solutions in Fig. 3b shows two differentiated shoulders overlapped with HER. The previous analyses conducted with nitrite allow clear assignment of each reduction peak to a specific overall reduction process. The first peak at −0.46 V vs RHE can be assigned to NO_3^- reduction to NO_2^- ($R_{NO_3^-}$), whereas the following peak (also observed in Fig. 3a) at a more negative potential of −0.87 V vs RHE corresponds to the subsequent reduction from NO_2^- to NH_3 ($R_{NO_2^-}$). Analysis of by-products yielded from potentiostatic reductions at these defined potentials confirmed that the main products formed are nitrite at −0.46 V vs RHE and ammonia at −0.87 V vs RHE (Fig. S7).

The higher current density registered for Cu/$Co(OH)_x$ electrodes in both NO_3^- and NO_2^- reductions can be related to the enhanced adsorbed hydrogen at the electrode surface. Previous studies confirm that cobalt-based structures present a high affinity for hydrogen dissociative adsorption during water splitting, yielding highly reductive monoatomic $H_{(ads)}$ [49]. The hydrogenation reaction of NO_3^- occurring along with direct charge transfer processes is a synergistic process still under exploration for nitrate reduction, but has been hypothesized by many authors (Cui et al., 2017; Liu et al., 2021; Xu et al., 2021; Yu et al., 2020). Indeed, the hydrogenation reaction contribution to overall NO_3^- reduction can be one of the reasons for the excellent performance displayed by noble metals such as Pt or Pd (Cerrón-Calle et al., 2022; Gauthard et al., 2003). One of the critical intermediates formed during the chemical and electrochemical reactions in nitrate reduction is the adsorbed *NO. This species is susceptible to react with adsorbed $H_{(ads)}$ on the electrode surface and steer the product selectivity towards ammonia through Eq. (15) or nitrogen gas through Eq. (16), respectively, depending on the N/H coverage ratio.

$$^*NO + 5H_{(ads)} \rightarrow {}^*NH_3 + H_2O \quad (15)$$

$$2^*NO + 4H_{(ads)} \rightarrow {}^*N_2 + 2H_2O \quad (16)$$

Thus, the HER should not only be considered as a competitive reaction, but also as an elemental process that can allow simultaneous catalytic hydrogenation reaction depending on the nature of the catalyst. For this reason, hydrogen adsorption was evaluated on Cu/$Co(OH)_x$ electrode to identify the effect of cobalt nanocomposites on the adsorbed hydrogen formed at the electrode surface. Cyclic voltammetry of bare Cu foam (Fig. 4a) presents no redox peaks associated with hydrogen adsorption. In contrast, Cu/$Co(OH)_x$ presents a new oxidation peak at 0.20 V vs RHE that only is registered when potentials where HER occurs are reached (Fig. 4b). The appearance of this peak is attributed to the oxidation of H_{ads}, which was adsorbed on the surface of $Co(OH)_x$ after HER. This analysis suggests that $Co(OH)_x$ as electrocatalyst may emulate the behavior of noble metals stabilizing $H_{(ads)}$ on their surface.

3.3. Performance of three-dimensional Cu/$Co(OH)_x$ electrodes on the electrochemical reduction of nitrate

The electrochemical reduction of nitrate was conducted under comparable conditions to benchmark the performance of pristine Cu foam (Fig. 5a) and Cu/$Co(OH)_x$ (Fig. 5b) electrodes. The time course of the concentration of N-species (mg L^{-1} as N) is depicted in Fig. 5. As can be observed, the gradual conversion of nitrate (NO_3^-) to nitrite (NO_2^-), ammonia (NH_3), and nitrogen species in the gas phase (N gas) occur for both materials but at different rates and selectivity. After 120 min, almost complete nitrate conversion (98.7 %) was attained by the Cu/$Co(OH)_x$ electrocatalyst ($k_1 = 6.0 \times 10^{-4}$ s^{-1}, $R^2 = 0.997$), while the Cu foam solely led to 55.3 % ($k_1 = 1.3 \times 10^{-4}$ s^{-1}, $R^2 = 0.988$). The Cu foam reached the highest amount of accumulated NO_2^- with 5.48 mg-N L^{-1} after 90 min, which decreased to 4.61 mg-N L^{-1} at the end of the treatment time. Conversely, the Cu/$Co(OH)_x$ led to a maximum concentration of NO_2^- of 1.61 mg-N L^{-1} after 15 min of reaction, which dropped down to 0.41 mg-N L^{-1} (value below the nitrite MCL of 0.90 mg-N L^{-1}) after 60 min of treatment, becoming completely negligible at the end of 120 min. These results agree with the higher electrocatalytic activity of Cu/$Co(OH)_x$ for nitrate and nitrite reduction as observed during the electroanalytical characterization.

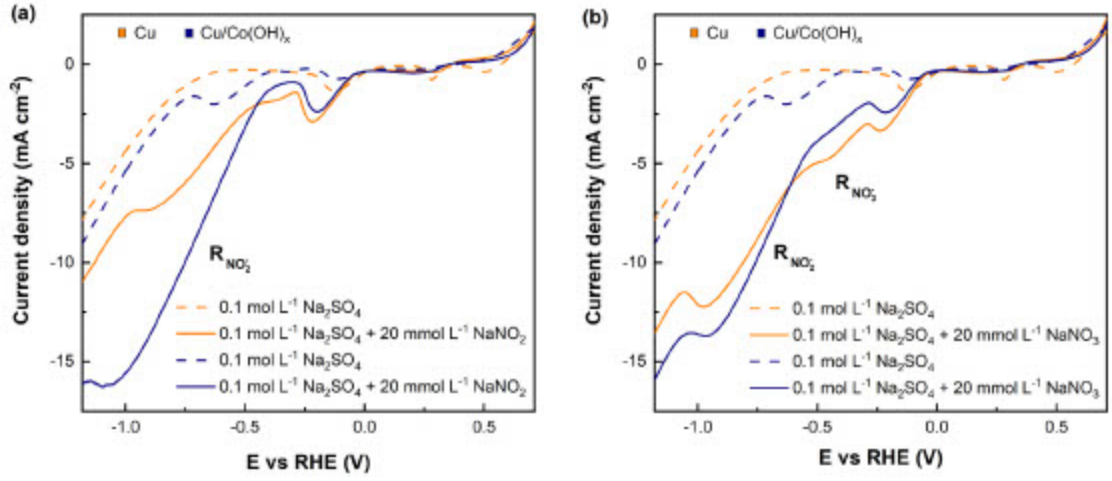

Fig. 3. Linear sweep voltammetry at 10 mV s^{-1} of Cu foam and Cu/$Co(OH)_x$ in a different solution of 0.1 mol L^{-1} Na_2SO_4 with (a) 20 mmol L^{-1} $NaNO_2$ and (b) 20 mmol L^{-1} $NaNO_3$.

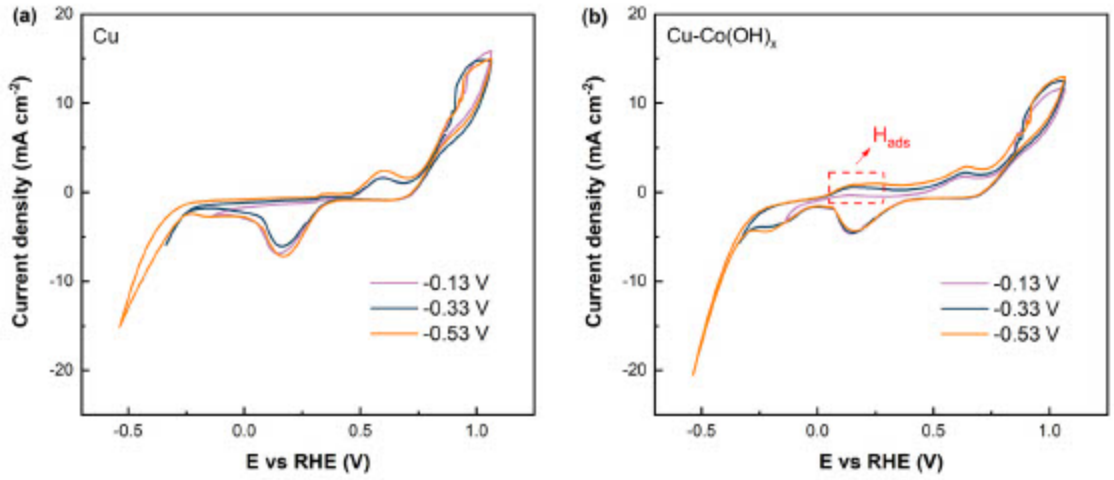

Fig. 4. Cyclic voltammetry at 25 mV s^{-1} of (a) Cu foam and (b) Cu/Co(OH)$_x$ in 0.1 mol L^{-1} NaOH (pH = 13) in different potential ranges from 1.05 V to −0.13, −0.33, and − 0.53 V vs RHE.

Product selectivity is essential to ensure maximum recovery of N-sources such as ammonia. While Cu foam allowed obtaining up to 11.36 mg-N L^{-1} after 120 min (Fig. 5a), the Cu/Co(OH)$_x$ attained 26.3 mg-N L^{-1} at 90 min (Fig. 5b), which is a 2.3 times higher concentration. However, a slight decrease in ammonia selectivity is observed on Cu/Co(OH)$_x$ electrode after 90 min of electrolysis resulting in decreased yield down to 24.0 mg-N L^{-1} at 120 min, which is probable due to the low amount of NO_3^- remaining in solution after 90 min of electrolysis.

Additionally, the electrochemical reduction of nitrite solutions was performed to study the reasons related to the shallow accumulation of nitrite from NO_3^- reduction when comparing Cu/Co(OH)x and pristine Cu electrodes performance. Fig. 6a and b correspond to the time course of N-species during the reduction of 30 mg-N L^{-1} of NO_2^- over 120 min. The NO_2^- constant kinetic decay (k_1) fitted well a pseudo-first-order reaction. As can be observed, using Cu/Co(OH)$_x$, the k_1 was 2-fold higher ($k_1 = 1.2 \times 10^{-3}\ s^{-1}$) than the value obtained with Cu foam ($k_1 = 0.6 \times 10^{-3}\ s^{-1}$). The nanocomposite Cu/Co(OH)$_x$ completely reduced nitrite in 60 min, while bare Cu required twice as long. These results demonstrated the catalytic effect of Co(OH)$_x$ sites that accelerate nitrite reduction to ammonia production.

The Co(OH)$_x$ sites provide the capability to increase the amount of H_{ads} in the electrode surface to reduce NO to NH_3 (Eq. (15)), which will explain the lower accumulation of nitrite during the NO_3^- electrolysis observed in Fig. 5b. It is well known that nitrite is a readily reducible species through catalytic hydrogenation while nitrate requires direct charge transfer (Hörold et al., 1993). Thus, the hydrogenation contribution may play a key role in expediting the reduced kinetics of formed nitrite, which will justify the lower nitrite accumulation observed for Cu/Co(OH)$_x$ electrodes. To evaluate the hydrogenation effect, nitrate reduction was assessed in the presence of tert-butyl alcohol (TBA) used as a H_{ads} scavenger (Gu et al., 2022). As can be seen in Fig. 7, the nitrate conversion rate significantly decreased after adding 10 and 20 mmol L^{-1} TBA. According to kinetic rate constant assessment, the contribution of hydrogen to the nitrate reduction was around 66.7 %, which is the double of the direct reduction contribution with a discrete 33.3 %. Furthermore, the influence of hydrogen on ammonia production was demonstrated by the decrease in ammonia production at higher TBA concentrations. These results show the outstanding performance of Co(OH)$_x$ in comparison with bare Cu to stabilize H_{ads} on the electrode surface for indirect reduction and ammonia production.

3.4. Assessing ammonia production and three-dimensional Cu/Co(OH)$_x$ electrode stability

The performance of the electrocatalytic system to obtain NH_3 was evaluated in terms of kinetic constants and figures of merit, such as

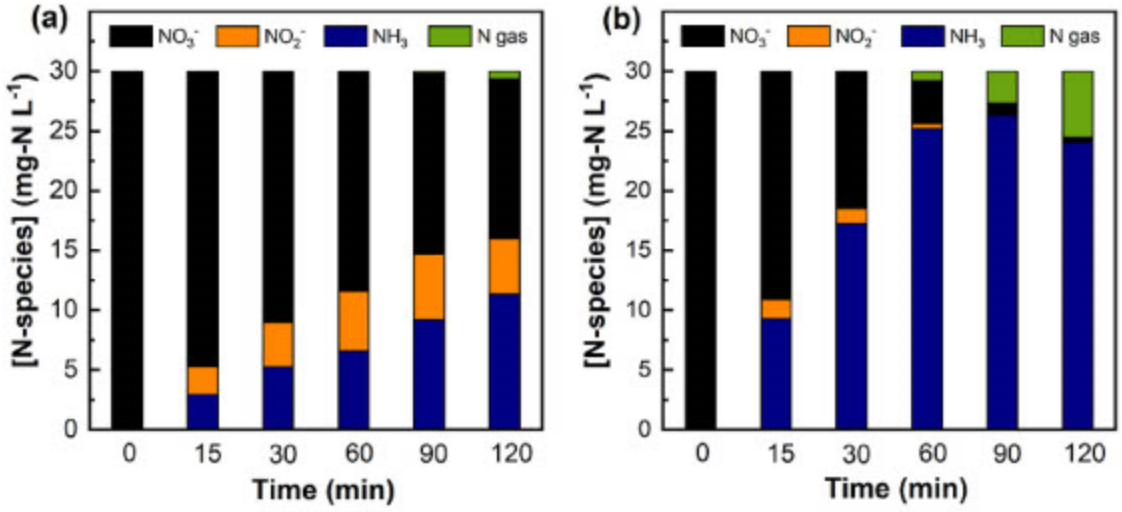

Fig. 5. Time-course of N-species (mg L^{-1}) for electrolysis of 30 mg NO_3^--N L^{-1} at 20 mA cm^{-2} using (a) Cu foam and (b) Cu/Co(OH)$_x$.

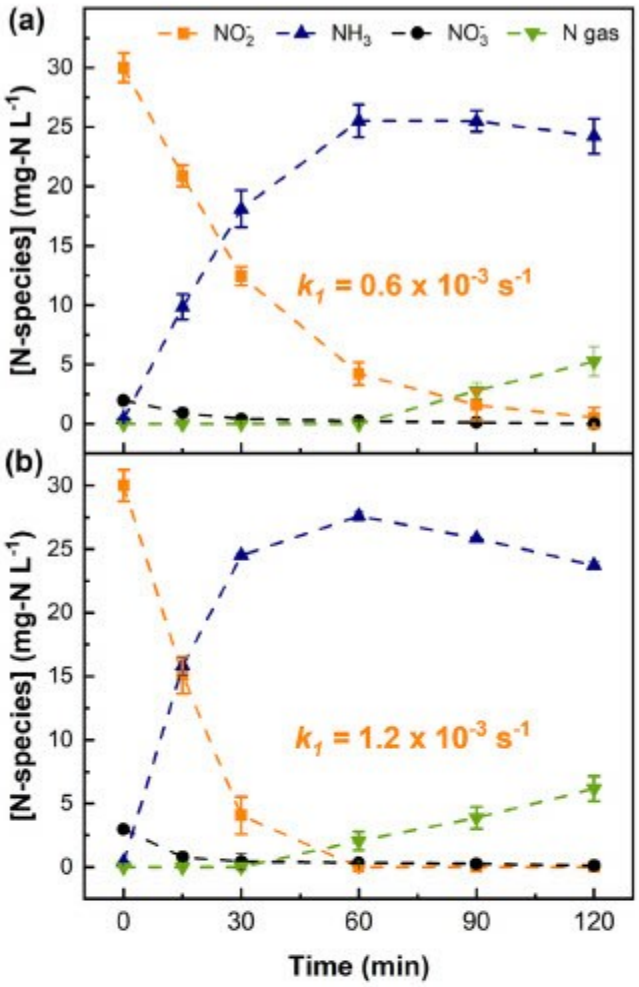

Fig. 6. The concentration of N-species over time for the electrolysis of 30 mg NO_2^--N L^{-1} using (a) Cu and (b) Cu/Co(OH)$_x$ electrodes at 20 mA cm^{-2}. Including the kinetic constant of NO_2^- reduction considering pseudo-first order reaction.

Faradaic efficiency (FE) and electrical energy per order (*EE/O*). The calculated pseudo-first-order kinetic constant for NO_3^- reduction of 6.0×10^{-4} s^{-1} for Cu/Co(OH)$_x$ was 4.6 times higher than the observed for pristine Cu foam ($k_1 = 1.3 \times 10^{-4}$ s^{-1}). These results demonstrated that the catalytic effect of Co(OH)$_x$ sites accelerate the nitrate abatement. Regarding figures of merit that describe energy requirements, 10.2 and 43.1 kWh m^{-3} order^{-1} *EE/O* values were obtained with Cu/Co(OH)$_x$ and Cu foam materials, respectively. For comparison, Fig. 8a includes the kinetic constant and *EE/O* obtained in our previous work using the bimetallic electrode Cu-Pt with 4.0×10^{-4} s^{-1} and 13.1 kWh m^{-3}, respectively (Cerrón-Calle et al., 2022). Under galvanostatic operation, the *EE/O* (Eq. 11) mostly depends on the observed cell potential and nitrate reduction kinetics. The observed cell potential is defined by the applied current density, the ohmic resistance of the system, and the electrode conductivity. Cell potentials (E_{cell}) at 20 mA cm^{-2} for Cu foam, Cu-Pt and Cu/Co(OH)$_x$ were 9.5 V, 8.8 V and 9.8 V, respectively. The three E_{cell} were under the same order of magniude, being in this case the kinetic rates, the main *EE/O* drivers. Cu/Co(OH)$_x$ shows the highest competitiveness, given the enhanced electrocatalytic performance on nitrate conversion kinetics. The low energy consumption for NH_3 production using environmental NO_3^- concentrations and bimetallic electrodes of Cu/Co(OH)$_x$ is more competitive than Pt plate operated under galvanostatic conditions in the literature (Fajardo et al., 2021). As displayed in Fig. 8b, Cu foam, and Cu/Co(OH)$_x$ showed an ammonia yield of 0.3 mmol NH_3 g_{cat}^{-1} h^{-1} and 0.7 mmol NH_3 g_{cat}^{-1} h^{-1}, respectively. Our previous research work with Cu-Pt bimetallic electrodes reported an ammonia yield of 0.6 mmol NH_3 g_{cat}^{-1} h^{-1}, which is higher than the Cu foam but lower than Cu/Co(OH)$_x$. Much higher ammonia yield values can be found in the literature working under potentiostatic conditions and using much higher NO_3^- initial concentrations (0.1–0.01 M NO_3^-), which makes impossible a proper comparison with our results (Fu et al., 2023; He et al., 2022; Li et al., 2022; Niu et al., 2022a, 2022b; Wang et al., 2023; Wu et al., 2022). The benefit of Cu/Co(OH)$_x$ goes beyond the higher productivity by setting a stepping stone in the path to substitute endangered and expensive PGM-based electrocatalysts. A meaningful performance indicator is the percentage of ammonia production referred to in terms of the maximum theoretical expected from the initial concentration of nitrate (Eq. (9)). Maximum ammonia production (100 %) would be attained if all initial nitrate concentration converts to ammonia. Fig. 8b depicts increasing values of ammonia production percentage of 38 %

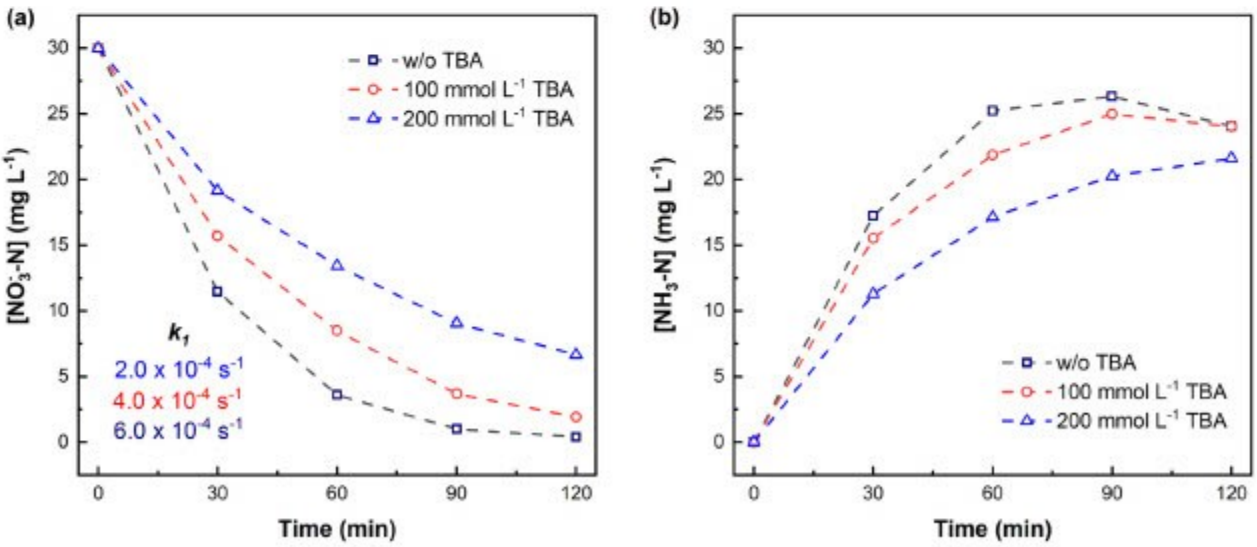

Fig. 7. (a) Nitrate reduction and (b) ammonia production as a function of time for Cu/Co(OH)$_x$ in the presence of different concentrations of TBA.

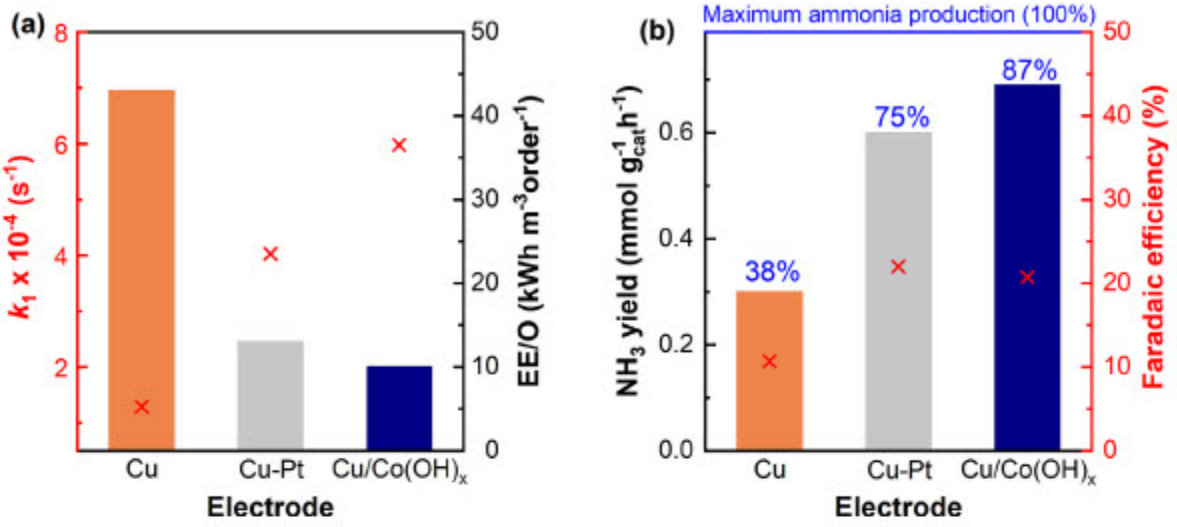

Fig. 8. (a) Electrical energy per order (bars) and kinetic constant for ammonia production (x) using Cu, Cu-Pt, and Cu/Co(OH)$_x$ electrodes. (b) Ammonia yield (bars) and Faradaic efficiency (x) after 120 min of electrolysis using Cu, Cu-Pt, and Cu/Co(OH)$_x$ electrodes. The numbers indicate the percentage of ammonia conversion from initial N-content.

(S_{NH_3} = 68 %), 75 % (S_{NH_3} = 84 %), and 87 % (S_{NH_3} = 81 %) for Cu foam, Cu-Pt, and Cu/Co(OH)$_x$, respectively.

The FE shows higher efficiency for both nanocomposites than for the pristine Cu. The Co(OH)$_x$ nanocomposites attained a 20.7 % FE, which is 2.0 times higher than the bare Cu foam. The observed FE of Cu/Co(OH)$_x$ had comparable values to those surveyed for noble electrocatalysts such as Cu-Pt (22.0 % FE). These are considered high FE for processes operated under galvanostatic conditions, which are lower than potentiostatic operation mode (Chen et al., 2020; Kapałka et al., 2011). However, galvanostatic electrolysis is the operational mode typically considered for scaled-up systems. These results identify Cu/Co(OH)$_x$ as a viable and competitive electrocatalyst for NH_3 production in low conductivity effluents.

Electrode activity and stability are essential parameters to determine the feasibility of scaling-up the electrocatalytic systems. Therefore, five sequential feed-batch trials were performed as a preliminary evaluation of the sustained performance of the Cu/Co(OH)$_x$ electrode under continuous operation. The effectiveness of the Cu/Co(OH)$_x$ electrode was evaluated regarding nitrate conversion and metal leaching after the five reuses. Fresh synthetic solutions containing nitrate were consecutively treated for 120 min under the same operating conditions. As shown in Fig. 9a, the Cu-Co(OH)$_x$ electrode presents an excellent reproducibility and sustained response over time. Identical abatement of initial nitrate concentration (98 % removal) was attained in consecutive runs showing identical kinetic rates. Thus, synthesized electrodes illustrate a resilient response and sustained electrocatalytic performance.

Metal leaching to aquatic mediums can be considered one of the main concerns of using multimetallic catalysts for water treatment. As reported by the National Primary Drinking Water Regulations (NPDWR), which is regulated by the United States Environmental Protection Agency (EPA), 1.3 mg L^{-1} is the maximum contaminant level (MCL) for copper and according to Europe Union (DOUE-L-2020-81,947) this maximum is set to 2.0 mg L^{-1}. Similar levels are set according to the emission standard pollutants for cobalt with an MCL around 50–100 µg L^{-1} (EU Drinking Water Directive (98/83/EC) and Republic of China GB25467–2010). Fig. 9b shows that the quantity of Cu (0.088–0.137 mg Cu L^{-1}) and Co (0.01–0.025 mg Co L^{-1}) leached after each use is significantly lower than the MCL by several orders of magnitude for both metals. The extraordinary activity and stability of the electrode can be attributed to its preparation method, since electrodeposition is an in-situ phenomenon that provides a strong attachment between material interfaces. This is superior to the physical attachment obtained by typical drop casting of nanomaterials. Therefore, it can be concluded that electrodeposition can generate stable electrodes for sustained performance of nitrogen management electrified systems.

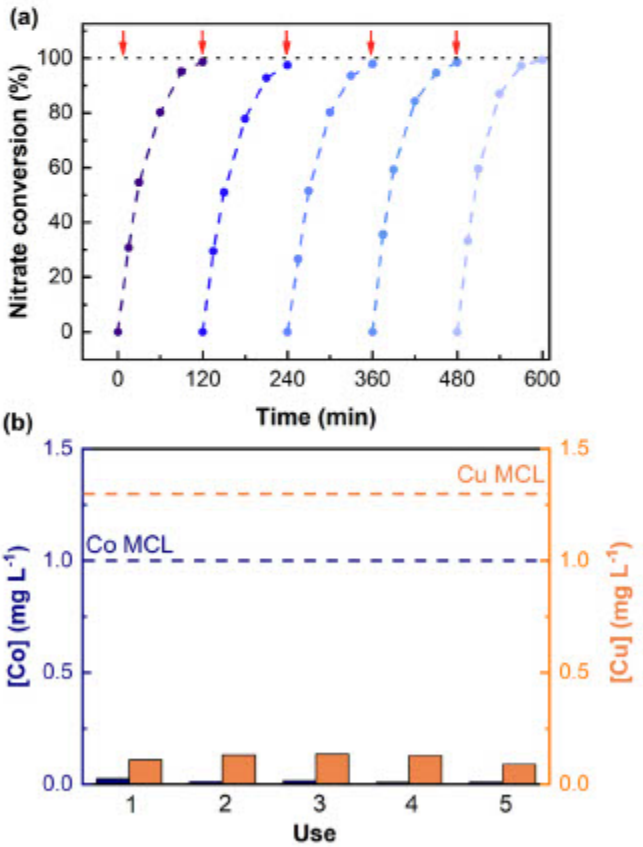

Fig. 9. (a) Nitrate conversion percentage during 5 consecutive experimental runs, arrows indicate solution renewal. (b) Copper and cobalt cations concentration remaining in solution after treatment. Dash lines presented the maximum contaminant level for each element.

4. Conclusion

Cobalt hydroxide nanocomposites electrodeposited over Cu foams were synthesized and tested for the electrochemical reduction of nitrate and ammonia production in a simulated low conductivity groundwater effluent. The cobalt hydroxide sites grown on the surface of the Cu foam modified the electrocatalytic response of the electrodes. This behavior is mainly due to the synergistic effect of Cu/Co$(OH)_x$ nano-interfaces that enable hybridized mechanisms of catalytic electrochemical and hydrogenation reduction processes. The new bimetallic active catalytic sites presented a higher nitrate conversion when compared to the pristine Cu electrode by overcoming the limiting step related to nitrate to nitrite initial reduction reaction. While the Cu surface promotes nitrate reduction to nitrite, Co$(OH)_x$ nanoparticles increase the conversion of nitrite to ammonia. After 120 min of treatment and under comparable operating conditions, Cu/Co$(OH)_x$ electrodes demonstrated an almost total nitrate conversion of 98.5 %. In contrast, the Cu foam electrode led to 55.4 %, corresponding to 1.2 times less. When benchmarking the earth-abundant Cu/Co$(OH)_x$ electrode with a Cu-Pt material, since no other Cu-Co electrocatalyst have been tested under galvanostatic conditions so far, the Cu/Co$(OH)_x$ electrodes reached the highest ammonia kinetics production ($k_1 = 6.0 \times 10^{-4}\ s^{-1}$, $R^2 = 0.997$) and ammonia yield (~ 0.7 mmol $g_{cat}^{-1}\ h^{-1}$), as well as the lowest *EE/O* with 10.2 kWh m^{-3} order^{-1}. Regarding the activity and stability of the new electrodes synthesized, the results were remarkable after 5 complete cycles of use, with no decrease in ERN performance efficiency, and the concentration of Cu and Co leached was always below the MCL. Therefore, this work on the electrocatalytic conversion of nitrate to ammonia has shown the great potential of bimetallic earth-abundant electrode materials to lead to an alternative and sustainable way for ammonia synthesis besides treating contaminated water streams containing nitrate. These systems provide a unique opportunity for a circular economy by enabling worldwide, decentralized ammonia recovery from polluted water sources. Another advantage of this setup is that it does not depend on fossil fuels and can be powered by renewable electricity from the sun, wind, and waves, reducing operational costs. This point is of great interest to developing countries that can use their natural renewable resources to support a more balanced/permanent ammonia production through green methods. Using earth-abundant materials as electrocatalysts, which global availability is not endangered, represents a game changer and a step forward for developing low-cost electrocatalytic-based treatment water systems. Identification of alternative electrocatalysts to cost-prohibitive PGMs can enable wide access to the technology for wider market implementation, given the drastic decrease in electrode cost. Experimental results evidenced even higher competitiveness than PGMs using the bimetallic earth-abundant combination in Cu/Co$(OH)_x$ electrodes. This work opens new avenues to explore alternative electrocatalyst combinations that were unexplored before, as well as defining new opportunities for the design of more compact reactors that explore the use of three-dimensional electrodes in flow-through configurations that increase the surface area per water volume treated using the same physical footprint than conventional flow-by electrochemical reactors.

Data availability

Data will be made available on request.

Declaration of competing interest

Authors declare no conflict of interest.

Acknowledgments

This material is based upon research supported by the Transatlantic Research Partnership of the Embassy of France in the United States and the FACE Foundation. The authors acknowledge the support of the Centre National de la Recherche Scientifique (CNRS). This work was partially funded by the National Science Foundation (NSF) through the Nanosystems Engineering Research Center for Nanotechnology-Enabled Water Treatment under project EEC-1449500. This project has received funding from the European Union's Horizon 2020 research and innovation program under the Marie Sklodowska-Curie grant agreement No 843870. The authors acknowledge Mr. Timothy Delazzer for assistance with preparing the TEM sample. J. L. acknowledges support by the National Science Foundation under Grant No. 1955474 (CHE-1955474). S.G.S acknowledges support by the Herman Frasch Fund for Chemical Research, Bank of America, N.A., Trustee. We acknowledge the use of facilities within the Eyring Materials Center at Arizona State University supported in part by NNCI-ECCS-1542160.

CRediT authorship contribution statement

G.A. C.-C. contributed conceptualization, methodology, validation, investigation, formal analysis, data curation, visualization, writing − original draft, writing − review & editing. **A.S.F.** contributed conceptualization, methodology, validation, investigation, formal analysis, data curation, visualization, writing − original draft, writing − review & editing, funding acquisition. **J.L.** contributed formal analysis, resources. **C.M.S.-S.** contributed conceptualization, methodology, formal analysis, resources, visualization, writing − original draft, writing − review & editing, supervision, funding acquisition. **S.G.-S.** contributed conceptualization, methodology, formal analysis, resources, visualization, writing − original draft, writing − review & editing, supervision, project administration, funding acquisition. All authors read and approved the final manuscript.

Appendix A. Supplementary data

Supplementary data to this article can be found online at https://doi.org/10.1016/j.scitotenv.2023.163938.

References

Atrashkevich, A., Fajardo, A.S., Westerhoff, P., Walker, W.S., Sánchez-Sánchez, C.M., Garcia-Segura, S., 2022. Overcoming barriers for nitrate electrochemical reduction: by-passing water hardness. Water Res. 225, 119118. https://doi.org/10.1016/j.watres.2022.119118.

Barley, M.H., Takeuchi, K.J., Meyer, T.J., 1986. Electrocatalytic reduction of nitrite to ammonia based on a water-soluble iron porphyrin. J. Am. Chem. Soc. 108, 5876–5885. https://doi.org/10.1021/ja00279a036.

Cerrón-Calle, G.A., Fajardo, A.S., Sánchez-Sánchez, C.M., Garcia-Segura, S., 2022. Highly reactive Cu-Pt bimetallic 3D-electrocatalyst for selective nitrate reduction to ammonia. Appl. Catal. B Environ. 302, 120844. https://doi.org/10.1016/j.apcatb.2021.120844.

Cerrón-Calle, G.A., Wines, A., Garcia-Segura, S., 2023. Atomic hydrogen provision by cobalt sites in a bimetallic Ni/Co(OH)x and trimetallic Ni/Cu2O/Co(OH)x configurations for superior ammonia production. Appl. Catal. B Environ. 328. https://doi.org/10.1016/j.apcatb.2023.122540.

Chen, G.F., Yuan, Y., Jiang, H., Ren, S.Y., Ding, L.X., Ma, L., Wu, T., Lu, J., Wang, H., 2020. Electrochemical reduction of nitrate to ammonia via direct eight-electron transfer using a copper–molecular solid catalyst. Nat. Energy 5, 605–613. https://doi.org/10.1038/s41560-020-0654-1.

Cui, Y., Zhou, C., Li, X., Gao, Y., Zhang, J., 2017. High performance electrocatalysis for hydrogen evolution reaction using nickel-doped CoS2 nanostructures: experimental and DFT insights. Electrochim. Acta 228, 428–435. https://doi.org/10.1016/j.electacta.2017.01.103.

Dai, X., Dai, Y., Lu, J., Pu, L., Wang, W., Jin, J., Ma, P., Tie, N., 2020. Cobalt oxide nanocomposites modified by NiCo-layered double hydroxide nanosheets as advanced electrodes for supercapacitors. Ionics 26, 2501–2511. https://doi.org/10.1007/s11581-019-03333-6 Kiel.

Deng, X., Yang, Y., Wang, L., Fu, X.Z., Luo, J.L., 2021. Metallic Co nanoarray catalyzes selective NH3 production from electrochemical nitrate reduction at current densities exceeding 2 a cm−2. Adv. Sci. 8, 1–9. https://doi.org/10.1002/advs.202004523.

Fajardo, A.S., Westerhoff, P., Sanchez-Sanchez, C.M., Garcia-Segura, S., 2021. Earth-abundant elements a sustainable solution for electrocatalytic reduction of nitrate. Appl. Catal. B Environ. 281, 119465. https://doi.org/10.1016/j.apcatb.2020.119465.

Flores, K., Cerrón-Calle, G.A., Valdes, C., Atrashkevich, A., Castillo, A., Morales, H., Parsons, J.G., Garcia-Segura, S., Gardea-Torresdey, J.L., 2022. Outlining key perspectives for the advancement of electrocatalytic remediation of nitrate from polluted waters. ACS ES&T Eng. 2, 746–768. https://doi.org/10.1021/acsestengg.2c00052.

Fu, W., Du, Y., Jing, J., Fu, C., Zhou, M., 2023. Highly selective nitrate reduction to ammonia on CoO/Cu foam via constructing interfacial electric field to tune adsorption of reactants. Appl. Catal. B Environ. 324, 122201. https://doi.org/10.1016/j.apcatb.2022.122201.

Gao, J., Jiang, B., Ni, C., Qi, Y., Bi, X., 2020. Enhanced reduction of nitrate by noble metal-free electrocatalysis on P doped three-dimensional Co3O4 cathode: mechanism exploration

from both experimental and DFT studies. Chem. Eng. J. 382, 123034. https://doi.org/10.1016/j.cej.2019.123034.
Gao, Y., Wang, Q., Ji, G., Li, A., 2022. Degradation of antibiotic pollutants by persulfate activated with various carbon materials. Chem. Eng. J. 429, 132387. https://doi.org/10.1016/j.cej.2021.132387.
Garcia-Segura, S., Lanzarini-Lopes, M., Hristovski, K., Westerhoff, P., 2018. Electrocatalytic reduction of nitrate: fundamentals to full-scale water treatment applications. Appl. Catal. B Environ. 236, 546–568. https://doi.org/10.1016/j.apcatb.2018.05.041.
Garcia-Segura, S., Nienhauser, A.B., Fajardo, A.S., Bansal, R., Conrad, C.L., Fortner, J.D., Marcos-Hernández, M., Rogers, T., Villagran, D., Wong, M.S., Westerhoff, P., 2020. Disparities between experimental and environmental conditions: research steps toward making electrochemical water treatment a reality. Curr. Opin. Electrochem. 22, 9–16. https://doi.org/10.1016/j.coelec.2020.03.001.
Gauthard, F., Epron, F., Barbier, J., 2003. Palladium and platinum-based catalysts in the catalytic reduction of nitrate in water: effect of copper, silver, or gold addition. J. Catal. 220, 182–191. https://doi.org/10.1016/S0021-9517(03)00252-5.
Glenn, S.M., James Lester, L., 2010. An analysis of the relationship between land use and arsenic, vanadium, nitrate and boron contamination in the Gulf Coast aquifer of Texas. J. Hydrol. 389, 214–226. https://doi.org/10.1016/j.jhydrol.2010.06.002.
Gu, Z., Zhang, Z., Ni, N., Hu, C., Qu, J., 2022. Simultaneous phenol removal and resource recovery from phenolic wastewater by electrocatalytic hydrogenation. https://doi.org/10.1021/acs.est.1c07457.
Guo, S., Li, H., Heck, K.N., Luan, X., Guo, W., Henkelman, G., Wong, M.S., 2022. Gold boosts nitrate reduction and deactivation resistance to indium-promoted palladium catalysts. Appl. Catal. B Environ. 305, 121048. https://doi.org/10.1016/j.apcatb.2021.121048.
Hamid, S., Niaz, Y., Bae, S., Lee, W., 2020. Support induced influence on the reactivity and selectivity of nitrate reduction by Sn-Pd bimetallic catalysts. J. Environ. Chem. Eng. 8, 103754. https://doi.org/10.1016/j.jece.2020.103754.
Hao, D., Wei, Y., Mao, L., Bai, X., Liu, Y., Xu, B., Wei, W., Ni, B.J., 2022. Boosted selective catalytic nitrate reduction to ammonia on carbon/bismuth/bismuth oxide photocatalysts. J. Clean. Prod. 331, 129975. https://doi.org/10.1016/j.jclepro.2021.129975.
Hasnat, M.A., Ben Aoun, S., Nizam Uddin, S.M., Alam, M.M., Koay, P.P., Amertharaj, S., Rashed, M.A., Rahman, M.M., Mohamed, N., 2014. Copper-immobilized platinum electrocatalyst for the effective reduction of nitrate in a low conductive medium: mechanism, adsorption thermodynamics and stability. Appl. Catal. A Gen. 478, 259–266. https://doi.org/10.1016/j.apcata.2014.04.017.
He, W., Zhang, J., Dieckhöfer, S., Varhade, S., Brix, A.C., Lielpetere, A., Seisel, S., Junqueira, J.R.C., Schuhmann, W., 2022. Splicing the active phases of copper/cobalt-based catalysts achieves high-rate tandem electroreduction of nitrate to ammonia. Nat. Commun. 13, 1–13. https://doi.org/10.1038/s41467-022-28728-4.
Hörold, S., Vorlop, K.D., Tacke, T., Sell, M., 1993. Development of catalysts for a selective nitrate and nitrite removal from drinking water. Catal. Today 17, 21–30. https://doi.org/10.1016/0920-5861(93)80004-K.
Ivanova, T.M., Maslakov, K.I., Sidorov, A.A., Kiskin, M.A., Linko, R.V., Savilov, S.V., Lunin, V.V., Eremenko, I.L., 2020. XPS detection of unusual Cu(II) to Cu(I) transition on the surface of complexes with redox-active ligands. J. Electron Spectros. Relat. Phenomena 238, 146878. https://doi.org/10.1016/j.elspec.2019.06.010.
Janoush, Z.A., Rezaee, A., Ghaffarinejad, A., 2020. Electrocatalytic nitrate reduction using Fe0/Fe3O4 nanoparticles immobilized on nickel foam: selectivity and energy consumption studies. J. Clean. Prod. 242, 118569. https://doi.org/10.1016/j.jclepro.2019.118569.
Juangsa, F.B., Irhamna, A.R., Aziz, M., 2021. Production of ammonia as potential hydrogen carrier: review on thermochemical and electrochemical processes. Int. J. Hydrog. Energy 46, 14455–14477. https://doi.org/10.1016/j.ijhydene.2021.01.214.
Jung, C., Sánchez-Sánchez, C.M., Lin, C.L., Rodríguez-López, J., Bard, A.J., 2009. Electrocatalytic activity of Pd-Co bimetallic mixtures for formic acid oxidation studied by scanning electrochemical microscopy. Anal. Chem. 81, 7003–7008. https://doi.org/10.1021/ac901096h.
Kapalka, A., Fierro, S., Frontistis, Z., Katsaounis, A., Neodo, S., Frey, O., De Rooij, N., Udert, K.M., Comninellis, C., 2011. Electrochemical oxidation of ammonia (NH4 + /NH 3) on thermally and electrochemically prepared IrO2 electrodes. Electrochim. Acta 56, 1361–1365. https://doi.org/10.1016/j.electacta.2010.10.071.
Katsounaros, I., 2021. On the assessment of electrocatalysts for nitrate reduction. Curr. Opin. Electrochem. 28, 100721. https://doi.org/10.1016/j.coelec.2021.100721.
van Langevelde, P.H., Katsounaros, I., Koper, M.T.M., 2021. Electrocatalytic nitrate reduction for sustainable ammonia production. Joule 5, 290–294. https://doi.org/10.1016/j.joule.2020.12.025.
Li, J., Zhan, G., Yang, J., Quan, F., Mao, C., Liu, Y., Wang, B., Lei, F., Li, L., Chan, A.W.M., Xu, L., Shi, Y., Du, Y., Hao, W., Wong, P.K., Wang, J., Dou, S.X., Zhang, L., Yu, J.C., 2020. Efficient ammonia electrosynthesis from nitrate on strained ruthenium nanoclusters. J. Am. Chem. Soc. 142, 7036–7046. https://doi.org/10.1021/jacs.0c00418.
Li, D., Gao, W., Geng, C., Meng, J., Guan, Y., Liang, J., Zhang, L., 2022. Low-nitrite generation Cu-Co/Ti cathode materials for electrochemical nitrate reduction. Environ. Sci. Pollut. Res., 18563–18576 https://doi.org/10.1007/s11356-022-23517-4.
Liang, Y., Zeng, Y., Tang, X., Xia, W., Song, B., Yao, F., Yang, Y., Chen, Y., Peng, C., Zhou, C., Lai, C., 2023. One-step synthesis of Cu(OH)2-Cu/Ni foam cathode for electrochemical reduction of nitrate. Chem. Eng. J. 451, 138936. https://doi.org/10.1016/j.cej.2022.138936.
Lin, Y.X., Zhang, S.N., Xue, Z.H., Zhang, J.J., Su, H., Zhao, T.J., Zhai, G.Y., Li, X.H., Antonietti, M., Chen, J.S., 2019. Boosting selective nitrogen reduction to ammonia on electron-deficient copper nanoparticles. Nat. Commun. 10, 1–7. https://doi.org/10.1038/s41467-019-12312-4.
Liu, A., Ming, J., Ankumah, R.O., 2005. Nitrate contamination in private wells in rural Alabama,United States. Sci. Total Environ. 346, 112–120. https://doi.org/10.1016/j.scitotenv.2004.11.019.
Liu, Y., Huang, B., Chen, X., Tian, Z., Zhang, X., Tsiakaras, P., Shen, P.K., 2020. Electrocatalytic production of ammonia: biomimetic electrode-electrolyte design for efficient electrocatalytic nitrogen fixation under ambient conditions. Appl. Catal. B Environ. 271. https://doi.org/10.1016/j.apcatb.2020.118919.
Liu, B., Cheng, Y., Cao, B., Hu, M., Jing, P., Gao, R., Du, Y., Zhang, J., Liu, J., 2021. Hybrid heterojunction of molybdenum disulfide/single cobalt atoms anchored nitrogen, sulfur-doped carbon nanotube /cobalt disulfide with multiple active sites for highly efficient hydrogen evolution. Appl. Catal. B Environ. 298, 120630. https://doi.org/10.1016/j.apcatb.2021.120630.
Lotfi, N., Shahrabi, T., Yaghoubinezhad, Y., Darband, G.B., 2020. Direct electrodeposition of platinum nanoparticles@graphene oxide@nickel-copper@nickel foam electrode as a durable and cost-effective catalyst with remarkable performance for electrochemical hydrogen evolution reaction. Appl. Surf. Sci. 505. https://doi.org/10.1016/j.apsusc.2019.144571.
MacFarlane, D.R., Cherepanov, P.V., Choi, J., Suryanto, B.H.R., Hodgetts, R.Y., Bakker, J.M., Ferrero Vallana, F.M., Simonov, A.N., 2020. A roadmap to the ammonia economy. Joule 4, 1186–1205. https://doi.org/10.1016/j.joule.2020.04.004.
Marcos-Hernández, M., Antonio Cerrón-Calle, G., Ge, Y., Garcia-Segura, S., Sánchez-Sánchez, C.M., Fajardo, A.S., Villagrán, D., 2022. Effect of surface functionalization of Fe3O4 nanoenabled electrodes on the electrochemical reduction of nitrate. Sep. Purif. Technol. 282, 119771. https://doi.org/10.1016/j.seppur.2021.119771.
Niu, Z., Fan, S., Li, X., Liu, Z., Wang, J., Duan, J., Tadé, M.O., Liu, S., 2022a. Facile tailoring of the electronic structure and the d-band center of copper-doped cobaltate for efficient nitrate electrochemical hydrogenation. ACS Appl. Mater. Interfaces 14, 35477–35484. https://doi.org/10.1021/acsami.2c04789.
Niu, Z., Fan, S., Li, X., Wang, P., Liu, Z., Wang, J., Bai, C., Zhang, D., 2022b. Bifunctional copper-cobalt spinel electrocatalysts for efficient tandem-like nitrate reduction to ammonia. Chem. Eng. J. 450, 138343. https://doi.org/10.1016/j.cej.2022.138343.
Price, J.G., 2011. Energy critical elements: securing materials for emerging technologies. Min. Eng. 63, 33–34.
Ren, T., Yu, Z., Yu, H., Deng, K., Wang, Z., Li, X., Wang, H., Wang, L., Xu, Y., 2022. Interfacial polarization in metal-organic framework reconstructed Cu/Pd/CuOx multi-phase heterostructures for electrocatalytic nitrate reduction to ammonia. Appl. Catal. B Environ. 318, 121805. https://doi.org/10.1016/j.apcatb.2022.121805.
Roy, A., Jadhav, H.S., Thorat, G.M., Seo, J.G., 2017. Electrochemical growth of Co(OH)2 nanoflakes on Ni foam for methanol electro-oxidation. New J. Chem. 41, 9546–9553. https://doi.org/10.1039/c7nj01929g.
dos Santos, A.J., Barazorda-Ccahuana, H.L., Caballero-Manrique, G., Chérémond, Y., Espinoza-Montero, P.J., González-Rodríguez, J.R., Jáuregui-Haza, U.J., Lanza, M.R.V., Nájera, A., Oporto, C., Pérez Parada, A., Pérez, T., Quezada, V.D., Rojas, V., Sosa, V., Thiam, A., Torres-Palma, R.A., Vargas, R., Garcia-Segura, S., 2023. Accelerating innovative water treatment in Latin America. Nat. Sustain. https://doi.org/10.1038/s41893-022-01042-z.
Shen, Z., Liu, D., Peng, G., Ma, Y., Li, J., Shi, J., Peng, J., Ding, L., 2020. Electrocatalytic reduction of nitrate in water using Cu/Pd modified ni foam cathode: high nitrate removal efficiency and N2-selectivity. Sep. Purif. Technol. 241. https://doi.org/10.1016/j.seppur.2020.116743.
Singh, S., Anil, A.G., Kumar, V., Kapoor, D., Subramanian, S., Singh, J., Ramamurthy, P.C., 2022. Nitrates in the environment: a critical review of their distribution, sensing techniques, ecological effects and remediation. Chemosphere 287, 131996. https://doi.org/10.1016/j.chemosphere.2021.131996.
Su, D., Xie, X., Munroe, P., Dou, S., Wang, G., 2014. Mesoporous hexagonal Co3O4 for high performance lithium ion batteries. Sci. Rep. 4. https://doi.org/10.1038/srep06519.
Teng, Y.G., Zuo, R., Xiong, Y., Wu, J., Zhai, Y.Z., Su, J., 2019. Risk assessment framework for nitrate contamination in groundwater for regional management. Sci. Total Environ. 697, 134102. https://doi.org/10.1016/j.scitotenv.2019.134102.
Tucker, P.M., Waite, M.J., Hayden, B.E., 2004. Electrocatalytic reduction of nitrate on activated rhodium electrode surfaces. J. Appl. Electrochem. 38, 781–796.
Wang, Yuhang, Xu, A., Wang, Z., Huang, L., Li, J., Li, F., Wicks, J., Luo, M., Nam, D.H., Tan, C.S., Ding, Y., Wu, J., Lum, Y., Dinh, C.T., Sinton, D., Zheng, G., Sargent, E.H., 2020. Enhanced nitrate-to-ammonia activity on copper-nickel alloys via tuning of intermediate adsorption. J. Am. Chem. Soc. 142, 5702–5708. https://doi.org/10.1021/jacs.9b13347.
Wang, Yuting, Zhou, W., Jia, R., Yu, Y., Zhang, B., 2020. Unveiling the activity origin of a copper-based electrocatalyst for selective nitrate reduction to ammonia. Angew. Chem. Int. Ed. 59, 5350–5354. https://doi.org/10.1002/anie.201915992.
Wang, C., Liu, Z., Dong, L., Du, F., Li, J., Chen, C., Ma, R., Li, C., Guo, C., 2023. Bimetallic CuCo nanocrystals to tailor absorption energy of intermediators for efficient electrochemical nitrate conversion to ammonia in neutral electrolyte. J. Power Sources 556, 232523. https://doi.org/10.1016/j.jpowsour.2022.232523.
Wu, W., Liu, J., Johannes, N., 2021. Electrodeposition of Ir–Co thin films on copper foam as high-performance electrocatalysts for efficient water splitting in alkaline medium. Int. J. Hydrog. Energy 46, 609–621. https://doi.org/10.1016/j.ijhydene.2020.09.268.
Wu, A., Zhou, Y., Lv, J., Zhang, D., Peng, Y., Ye, Q., Fu, P., Wang, W., Lin, X., Liu, S., Xu, M., Qi, Z., Zhu, S., Zhu, W., Yan, J., Tu, X., Li, X., 2022. Boosting electrocatalytic nitrate-to-ammonia conversion via plasma enhanced CuCo alloy-substrate interaction. ACS Sustain. Chem. Eng. 10, 14539–14548. https://doi.org/10.1021/acssuschemeng.2c04249.
Xiao, Z., Huang, Y.C., Dong, C.L., Xie, C., Liu, Z., Du, S., Chen, W., Yan, D., Tao, L., Shu, Z., Zhang, G., Duan, H., Wang, Y., Zou, Y., Chen, R., Wang, S., 2020. Operando identification of the dynamic behavior of oxygen vacancy-rich Co3O4for oxygen evolution reaction. J. Am. Chem. Soc. 142, 12087–12095. https://doi.org/10.1021/jacs.0c00257.
Xu, B., Chen, Z., Zhang, G., Wang, Y., 2021. On-demand atomic hydrogen provision by exposing electron-rich cobalt sites in an open-framework structure toward superior electrocatalytic nitrate conversion to dinitrogen. Environ. Sci. Technol. https://doi.org/10.1021/acs.est.1c06091.
Yang, L., Li, J., Du, F., Gao, J., Liu, H., Huang, S., Zhang, H., Li, C., Guo, C., 2022. Interface engineering cerium-doped copper nanocrystal for efficient electrochemical nitrate-to-ammonia production. Electrochim. Acta 411, 140095. https://doi.org/10.1016/j.electacta.2022.140095.
Yu, Yu., Wang, C., Yu, Yifu, Wang, Y., Zhang, B., 2020. Promoting selective electroreduction of nitrates to ammonia over electron-deficient Co modulated by rectifying Schottky contacts. Sci. China Chem. 63, 1469–1476. https://doi.org/10.1007/s11426-020-9795-x.